PL-TR-93-2132 (I)

CHARACTERIZATION OF THE ENERGY DEPOSITION PRODUCED BY THE PRIMARY ELECTRON BEAM ON THE EXCEDE III PROGRAM

R.J. Rieder
R.L. McNutt, Jr.
S.A. Rappaport

Visidyne, Inc.
10 Corporate Place
South Bedford Street
Burlington, MA 01803

May 1993

Scientific Report No. 3

PHILLIPS LABORATORY
Directorate of Geophysics
AIR FORCE MATERIEL COMMAND
HANSCOM AIR FORCE BASE, MA 01730-3010

This technical report has been reviewed and is approved for publication

FRANCIS X. ROBERT
Contract Manager

STEPHAN D. PRICE
Branch Chief

ROGER VAN TASSEL
Division Director

This report has been reviewed by the ESC Public Affairs Office (PA) and is releasable to the National Technical Inf rmation Service (NTIS).

Qualified requestors may obtain additional copies from the Defense Technical Information Center. All others should apply to the National Technical Information Service.

If your address has changed, or if you wish to be removed from the mailing list, or if the addressee is no longer employed by your organization, please notify PL/TSI, Hanscom AFB, MA 01731-3010. This will assist us in maintaining a current mailing list.

Do not return copies of this report unless contractual obligations or notices on a specific document requires that it be returned.

REPORT DOCUMENTATION PAGE

Form Approved
OMB No. 0704-0188

1. AGENCY USE ONLY (Leave Blank)	2. REPORT DATE	3. REPORT TYPE AND DATES COVERED
	May 1993	Scientific Report No. 3

4. TITLE AND SUBTITLE
Characterization of the Energy Deposition Produced by the Primary Electron Beam on the EXCEDE III Program

5. FUNDING NUMBERS
PE 63220C
PR S321 - TA 06 - WU AB
Contr. F19628-90-C-0187

6. AUTHOR(S)
R.J. Rieder
R.L. McNutt *
S.A. Rappaport

7. PERFORMING ORGANIZATION NAME(S) AND ADDRESS(ES)
Visidyne, Inc.
10 Corporate Place
South Bedford Street
Burlington MA 01803

8. PERFORMING ORGANIZATION REPORT NUMBER
VI-2067

9. SPONSORING/MONITORING AGENCY NAME(S) AND ADDRESS(ES)
Phillips Laboratory
29 Randolph Road
Hanscom AFB, MA 01731-2010

Contract Manager: Frank Robert/GPOB

10. SPONSORING/MONITORING AGENCY REPORT NUMBER
PL-TR-93-2132 (I)

11. SUPPLEMENTARY NOTES

* Applied Physics Lab, Johns Hopkins University, Laurel, MD

12a. DISTRIBUTION/AVAILABILITY STATEMENT

Approved for Public Release; Distribution Unlimited

12b. DISTRIBUTION CODE

13. ABSTRACT *(Maximum 200 words)*

The primary goal of the EXCEDE III (Excitation by Electron Deposition) atmospheric energy deposition experiment was to monitor the spatial distribution of the energy deposition profile produced by the ~18 Ampere ~2.5 keV electron beam. During the rocket flight on April 27, 1990, prompt emission at 3914 Å from the N_2^+ (1N) 0-0 transition were measured by a UV scanning photometer. We have inverted the intensity profiles to obtain profiles of energy deposition by the beam.

14. SUBJECT TERMS

EXCEDE III, N^+_2 (IN), 3914 Å, Electron Beam, Atmospheric Deposition, Artificial Aurora, Scanning Photometer

15. NUMBER OF PAGES
38

16. PRICE CODE

17. SECURITY CLASSIFICATION OF REPORT	18. SECURITY CLASSIFICATION OF THIS PAGE	19. SECURITY CLASSIFICATION OF ABSTRACT	20. LIMITATION OF ABSTRACT
Unclassified	Unclassified	Unclassified	SAR

Table of Contents

List of Figures

Acknowledgements

The EXCEDE III effort at Visidyne was supported by the Geophysics Directorate of the Air Force Phillips Laboratory (PL/GPOA) via contract F19628-90-C-0187 with Visidyne, Inc. This work is sponsored by the Defense Nuclear Agency under DNA MIPR #93-530, and Work Unit 00029.

Introduction

EXCEDE III (Excitation by Electron Deposition) is an atmospheric energy deposition rocket experiment which was launched on 27 April 1990 from White Sands Missile Range. Included as part of the EXCEDE II sensor module ("daughter") payload were several photometers with a mechanically scanned mirror. The purpose of these instruments was to obtain spatial profiles of the beam intensity at a variety of wavelengths and at a fixed angular distance along the beam from the accelerator module. One of these photometers was filtered to respond to light at 3914 Å.

Emissions at 3914 Å result from the excitation of the (0,0) first negative band of N^+_2 [denoted N_2^+ (1N) *Borst and Zipf*, 1970]. The excited state produced by electron impact is $B^2\ \Sigma^+_u$ which has a lifetime of 70 ns [*Jones*, 1971] and decays to $X^2\ \Sigma^+_g$. This excitation has a threshold energy of 18.8 eV, a peak cross section at 100 eV, and a slow decrease in the cross section toward higher energies [*Borst and Zipf*, 1970]. These factors make emissions at this wavelength an excellent indicator of the spatial extent of energy deposition by the primary beam. Monitoring of this line has been a standard diagnostic tool in auroral observations.

Experiment Goals

The primary goal for the scanning photometer investigations was to obtain the spatial distribution of energy deposited in the upper atmosphere by the EXCEDE III beam. The technique employed the 3914 Å emission as a deposition diagnostic (also used in the characterization of natural aurora). The narrow-band photometer ($\sim$ 13 Å FWHM) was scanned from -15° (ahead of the beam) to +30° (trailing the beam) across the nominal beam location at $\sim$ 1 scan per second. The measured field of view for this photometer is $\sim$0.1°. The viewing geometry is shown schematically in Figure 1. A variety of other infrared, visible, and ultraviolet photometers and spectrometers were also used to measure intensities at the beam and in the afterglow region. The results of these studies will be presented elsewhere.

The scanning photometer experiment package was designed and assembled at Visidyne and consists of four photometers with narrow band filters, a motor-driven scanning mirror, the optics assembly and associated electronics. A schematic drawing of the instrument is shown in Figure 2.

The 3914 Å photometer consisted of a EMI 541N photomultiplier tube (PMT) in conjunction with an aperture, a lens, and a narrow band filter. The sensor was limited to maximum counting rates of $\sim 2 \times 10^6$ counts/second and had dark noise counts of 38 per second. As mentioned above, the narrow band filters have characteristic widths (FWHM) of $\sim$13 Å. Recent measurements of these same transmission curves show that the spectral response of the filter has remained stable two years after the flight.

In spite of the relatively high emission intensity of the beam, the number of counts in each measurement bin are relatively low during many of the scans near apogee because the integration

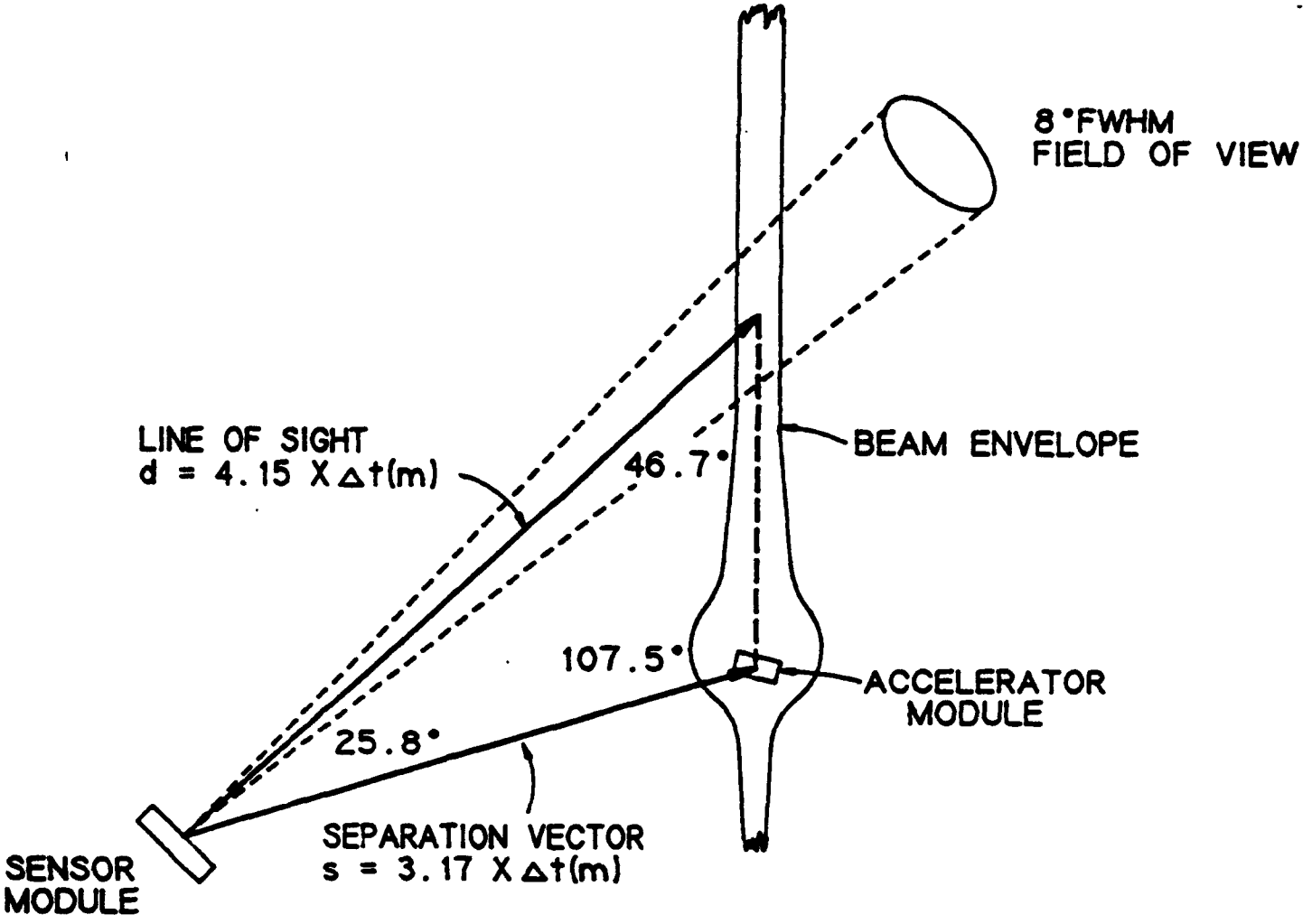

Figure 1.: Viewing geometry of the sensor module with respect to the accelerator module.

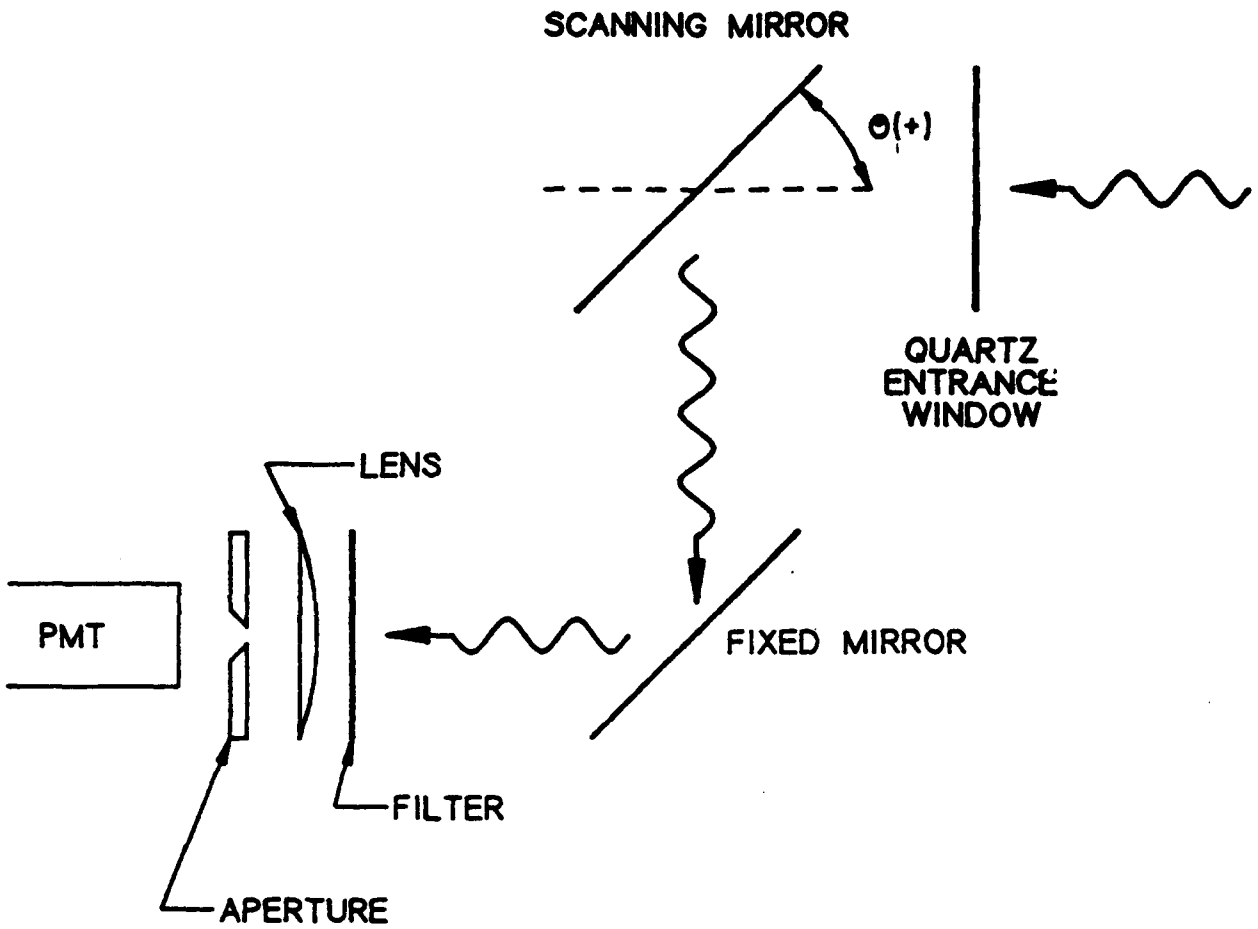

Figure 2.: Schematic drawing of the EXCEDE III scanning photometer.

time per measurement is short (1.33 ms). The instrument count rate was set by the need for minimizing the uncertainties due to counting statistics while maximizing the spatial resolution across the beam.

In addition to the photometer centered on 3914 Å, the unit also included narrow-band photometers centered on 3805 Å ($N_2(2P)$ $\nu'=0,\nu''=2$), 5577 Å ($^1S_0$ - $^1D_2$ "auroral green line"), and 2761 Å (N_2 Vegard Kaplan (0,6) transition). Both of the excited states for the latter two emissions are long-lived. The emissions measured by these photometers trace out the evolution of the region into which the beam energy is deposited and will be discussed elsewhere.

Experimental Results

There were 170 scans made by the 3914 Å photometer between 133 s (after launch) and 300 seconds, including 90 scans with the electron beam on. We have analyzed the beam-on scans in terms of a generalized Gaussian function (described below) plus a background count rate. The beam-off scans were used only to determine a background photon count rate.

In the 3914 Å data there is an asymmetry in the scan profiles early in the flight which develops into a second completely separated peak by the time of 165 seconds. The secondary peak always appears on the side of the primary peak that is "downstream" with respect to the motion of the two modules through the ionosphere. The ratios of the areas under the two intensity curves varies from ~ 5 to $\sim 10\%$; the widths are similar (although less well-determined for the secondary peak). The *angular* separation of the two remains relatively constant at 1.75°. This latter constancy of angle suggested that the second peak could be an instrumental artifact (F. Bien, private communication).

Subsequent to this suggestion, the flight photometer unit was set up in the laboratory to test this hypothesis (the instrument payload on the Sensor Module was recovered after successful parachute deployment). A calibrated NIST source lamp employing a halogen-quartz envelope and coiled-coil filament was used to produce an extended source by illuminating a diffusion screen. The screen was then masked to look like a spatial line source similar to the EXCEDE III beam (full width $\sim 0.75°$). The source was then scanned with the flight unit mirror with the intensity from the 3914 Å photometer recorded. A schematic of the laboratory setup is shown in Figure 3. This laboratory simulation revealed a secondary peak with an integrated area of 10% of the primary peak and at an angular separation of 1.68°. Further investigation has shown that the extra peak in the 3914 Å data can be traced to a reflection due to the narrow-band filter assembly.

The effects of the reflection on the flight data are minimal and do not compromise any of the results. Because the reflection always occurs on the same side of the scan, the leading edge of all the scans are not affected. The data are fit to a symmetric function and as can be seen in Figure 4 the unaffected edge of the fit is in excellent agreement with the data. Where possible, we have fit the data to a two-peak intensity distribution and then analyzed the parameters of the primary peak alone to determine the energy deposition properties of the beam.

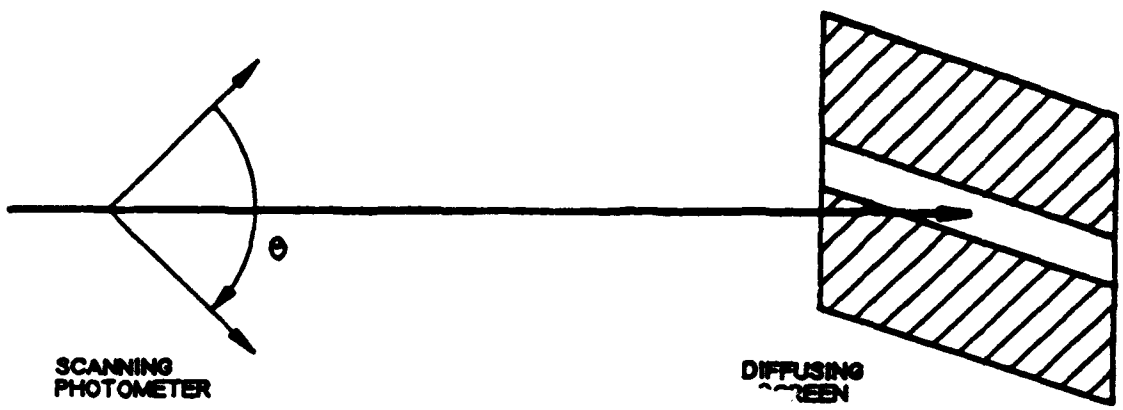

LABORATORY SETUP

Figure 3.: Schematic of post calibration laboratory setup.

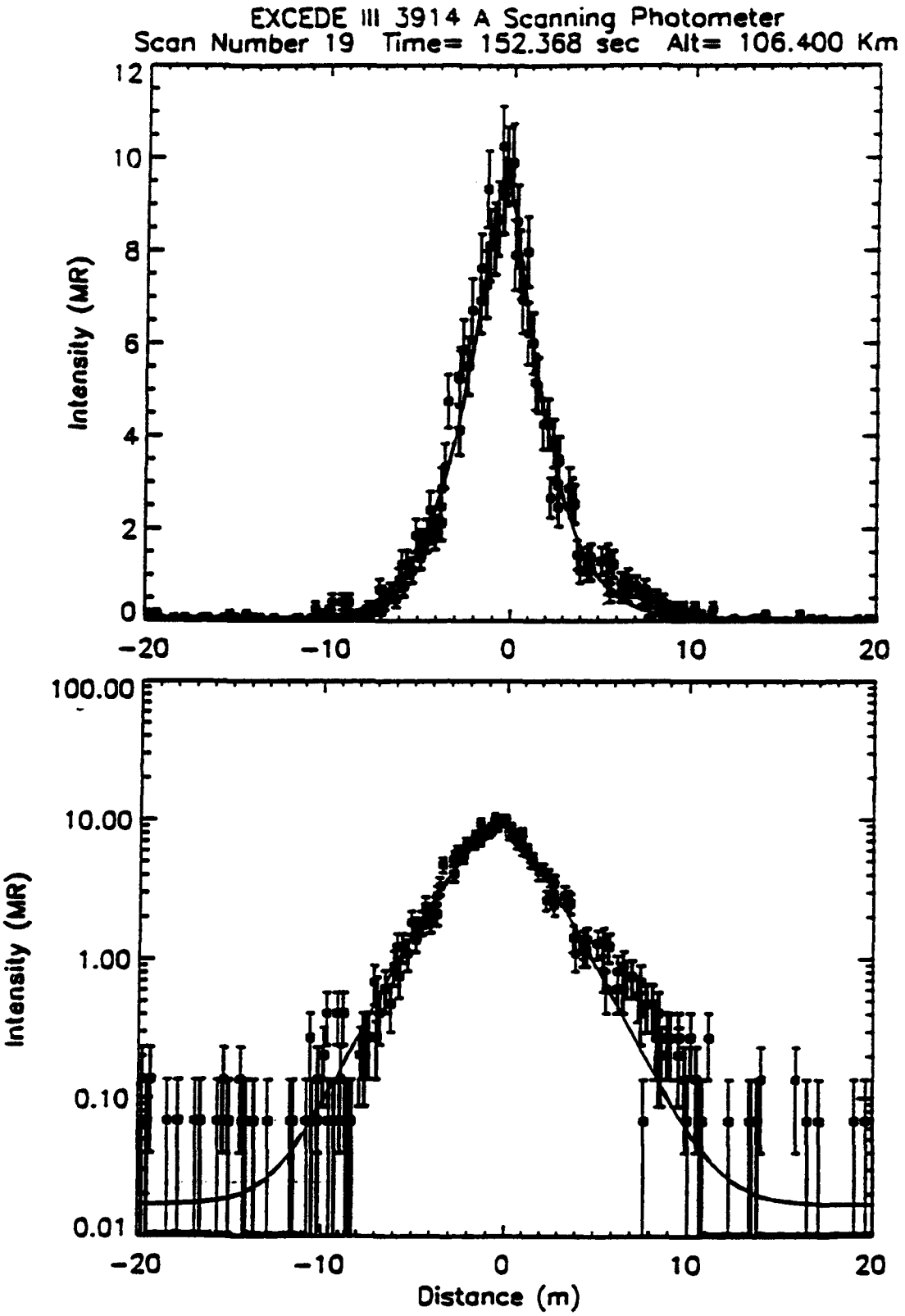

Figure 4.: 3914 Å scanning photometer scan number 19.

Unfolding the Deposition Profile. Let $\rho(r)$ be the volume emissivity of the beam, where r is the distance from the beam axis to the differential volume of emission in cylindrical coordinates. Here we assume that the emission pattern (with the secondary peak eliminated) has cylindrical symmetry. Let the x-axis be defined by a line along the instantaneous view direction of the photometer, let the y-axis be along the direction perpendicular to the x-axis and through the nominal center of the beam, and let the z-axis be coplanar with the symmetry axis of the beam. We assume that the observer is located a distance r from the nominal beam center and that the x-axis makes an angle Θ to the beam axis; the geometry is indicated in Figure 5. The distance y is then related to the photometer mirror scan angle ϕ by

$$y = R \sin \phi \tag{1}$$

If $\Sigma'(y)$ is the measured intensity, and Σ is the intensity that would be observed perpendicular to the beam axis, then we have

$$\Sigma(y) = \Sigma'(y) \sin \theta \tag{2}$$

and

$$\Sigma(y) = \int_{-\infty}^{+\infty} \rho(x,y)\, dx \tag{3}$$

where $r^2 = x^2 + y^2$. Equivalently

$$\Sigma(y) = \int_{y}^{+\infty} \frac{r\, \rho(r)}{\sqrt{r^2 - y^2}}\, dr \tag{4}$$

where we have made use of the assumed cylindrical symmetry by writing $\rho(r)$ for $\rho(x,y)$.

The volume emissivity is given by the solution of eqn. (4), which is a Volterra integral equation first studied by Abel [*Courant and Hilbert*, 1953]. The solution leads to the Abel transform, which is encountered in unfolding projected luminosity functions in a variety of settings [*Bracewell*, 1956, *Press et al.*, 1976]. The emissivity ρ is given by the inverse Abel transform [e.g., *Bracewell*, 1956]

$$\rho(r) = -\frac{1}{\pi} \int_{r}^{\infty} \frac{\frac{d}{dy}[\Sigma(y)]\, dy}{\sqrt{y^2 - r^2}} \tag{5}$$

Generalized Gaussian Distribution. The statistical noise in the data precludes the direct application of the inversion in Eqn. (5). What can be inverted is an analytic form for $\Sigma(y)$

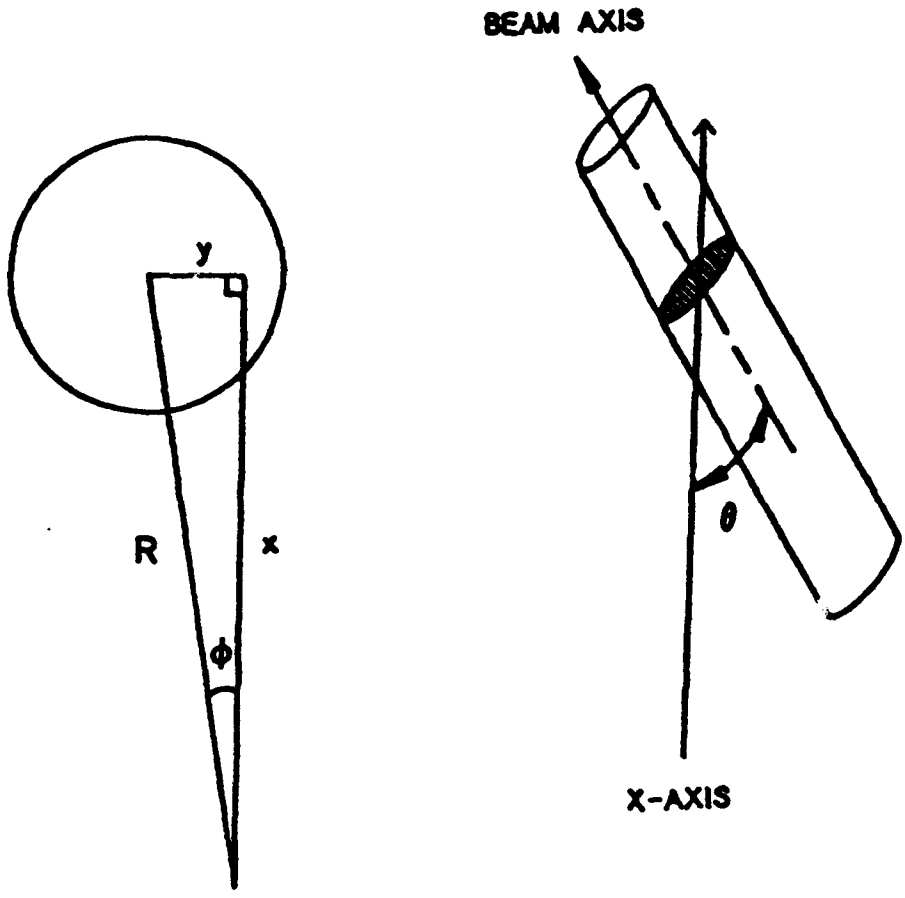

Figure 5.: Geometry diagram for deposition analysis.

which includes a sufficient number of parameters to characterize the data well. These parameters (plus their statistical uncertainties) can then be obtained by solving the "forward problem" in a least squares sense (e.g., [*Bevington*, 1969]).

As a first cut to the interpretation of the 3914 Å data we have found a convenient analytic function for fitting the intensity scans to be a "generalized gaussian" defined by [*Tarantola*, 1987]

$$\Sigma_p(y) \equiv A_\Sigma \sin\theta \frac{p^{1-1/p}}{2\sigma\,\Gamma(1/p)} \exp\left[-\frac{1}{p}\frac{|y-y_o|^p}{\sigma^p}\right] \tag{6}$$

with

$$\int_{-\infty}^{+\infty} \Sigma_p(y)\,dy = A_\Sigma \sin\theta \tag{7}$$

and where y_o is the center of the distribution, σ is a measure of the width, and p is the power in the generalized Gaussian (for p=2 the distribution reduces to a simple Gaussian). By using a generalized Gaussian for $\Sigma(y)$ measured from the symmetry point, i.e., putting $y_o = 0$ we obtain

$$\rho(r) = \frac{1}{\pi}\frac{A_\Sigma \sin\theta}{\Gamma(1/p)}\left[\frac{p}{2}\right]\frac{1}{(p^{1/p}\,\sigma)^2} f_p(\alpha) \tag{8}$$

where

$$\alpha \equiv \left[\frac{r}{p^{1/p}\,\sigma}\right]^p \tag{9}$$

and

$$f_p(\alpha) \equiv \int_\alpha^\infty \frac{e^{-z}\,dz}{\sqrt{z^{2/p}-\alpha^{2/p}}} \tag{10}$$

or, equivalently,

$$f_p(\alpha) = p\,\alpha^{1-1/p}\int_0^\infty e^{-\alpha\cosh^p v}\cosh^{p-1}v\,dv \tag{11}$$

In general $f_p(\alpha)$ cannot be evaluated in terms of simpler functions; however, there are simple forms for the following special cases

$$f_1(\alpha) = K_o(\alpha) \tag{12}$$

$$f_2(\alpha) = \sqrt{\pi}\, e^{-\alpha} \tag{13}$$

$$f_p(0) = \Gamma(1 - 1/p) \qquad for\ p > 1 \tag{14}$$

3914 Å Individual Scans. The 90 scans made by the 3914 Å photometer with the electron beam on have been fit to a generalized gaussian with the parameters: A_Σ ≡ integrated intensity (Megarayleigh - meter); y_o ≡ center location (meter); σ ≡ width (meter); p ≡ generalized exponent; and I_o = constant background. The beam-off scans were averaged to compute a noise level. Plots of the five fitted parameters are displayed in Figures 6 - 10 as a functions of time.

Figure 6 is a plot of the amplitude, A_Σ, in units of MR-meters. A_Σ is equal to the area under the generalized gaussian and represents the total number of 3914 Å photons emitted from the scanned slice of the beam. The distribution of amplitudes is approximately symmetric about 195 seconds (apogee) where the values are close to minimum. The 3914 Å intensity is characterized by the atmospheric density being largest at times corresponding to lower altitudes and smallest at higher altitudes. The two clusters of low points (centered at 208 and 215 seconds) correspond to gun cycles 13 and 14 where the gun currents were reduced due to load faults in the accelerator system.

The generalized exponent, p, is plotted in Figure 7. From the plot, we can see that a typical value for p lies between 1.3 and 1.8. The value of these exponents infers that the beam is more peaked at its center than would be the case for a standard gaussian distribution (i.e. p=2).

The location of the center of the beam is plotted in Figure 8 in units of degrees and meters. A value of zero indicates that the center of the interferometer FOV (from which all instrument directions are referenced) is centered on the beam. Positive (negative) values of y_o correspond to the center of the interferometer being aimed ahead of (behind) of the beam. The derived centroids indicate that the interferometer is initially aimed ahead of the beam by a few degrees and becomes more nearly centered up to ~250 seconds.

The width of the generalized Gaussian, σ (see eqn. 6), is also plotted in units of both degrees and meters in Figure 9. The value of σ stays relatively constant at ~2.3 meters over the entire upleg of the flight and then steadily increases to over 4 meters at 250 seconds. Note, however, that in terms of angular size σ remains essentially constant at 0.35 degrees through the downleg. However, because the generalized exponent can also change, the width of the beam is better characterized by the RMS diameter described in the following section.

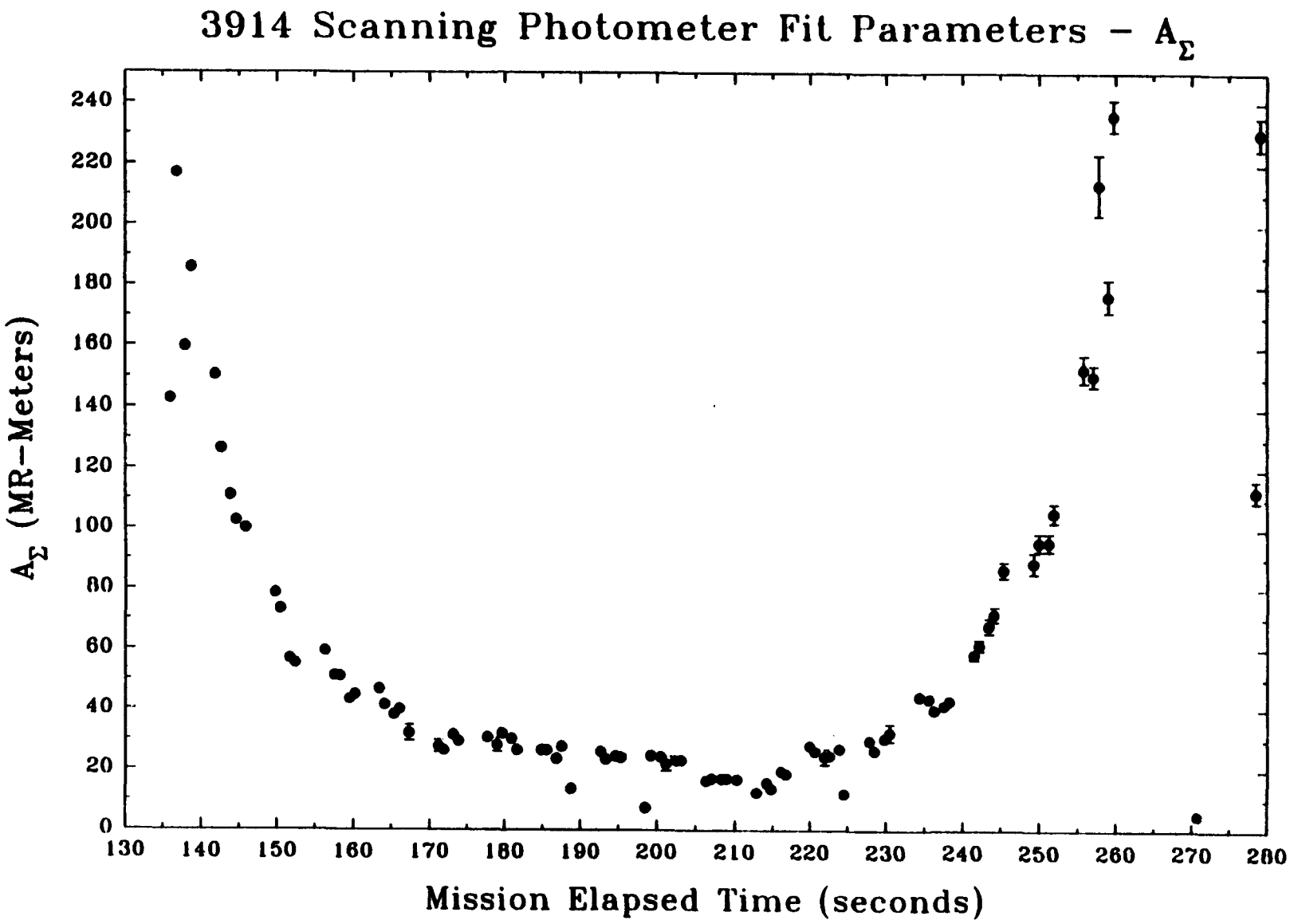

Figure 6. 3914 Å scanning photometer fit parameters - amplitude.

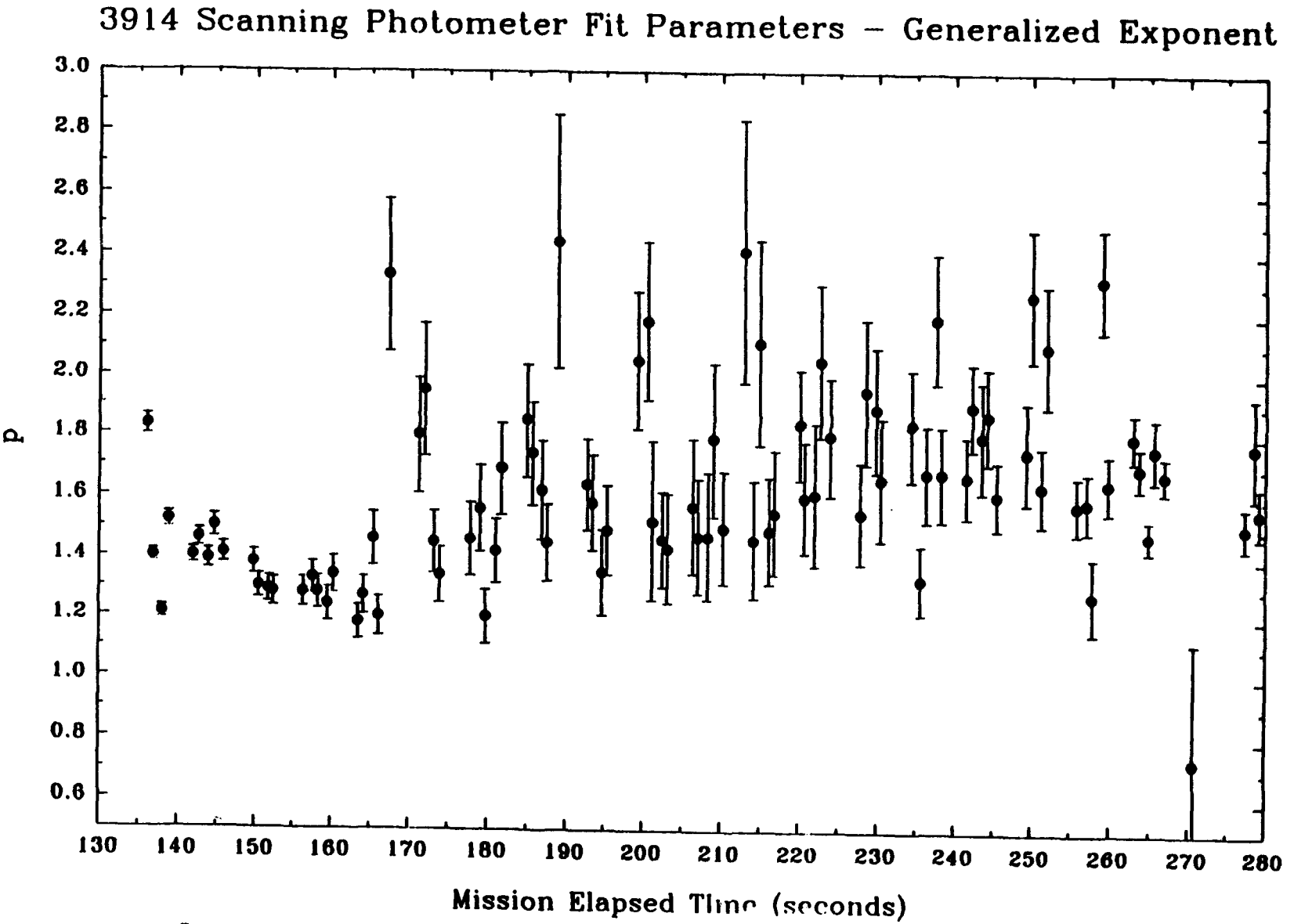

Figure 7. 3914 Å scanning photometer fit parameters - generalized exponent.

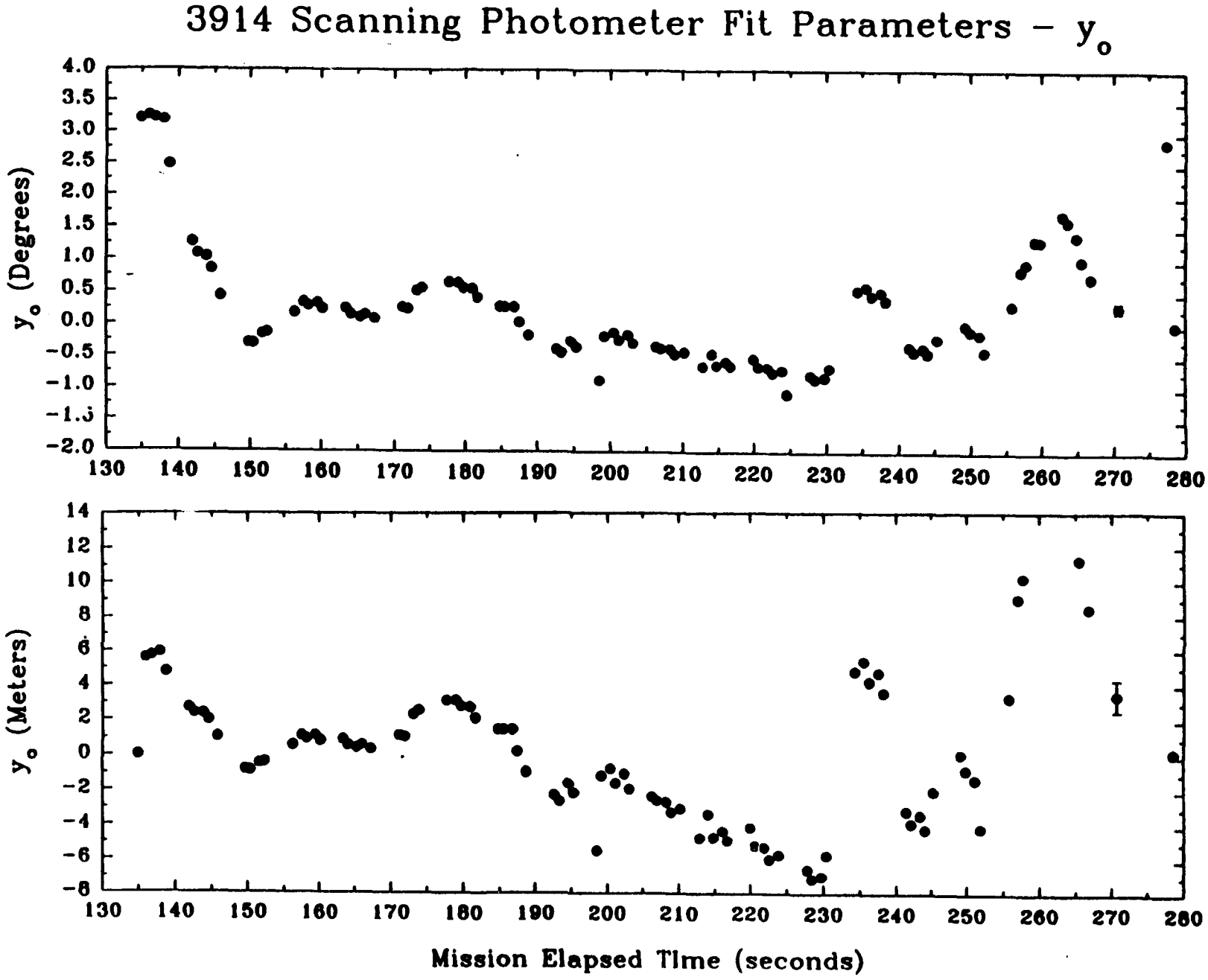

Figure 8. 3914 Å scanning photometer fit parameters - centroid (in units of meters and degrees).

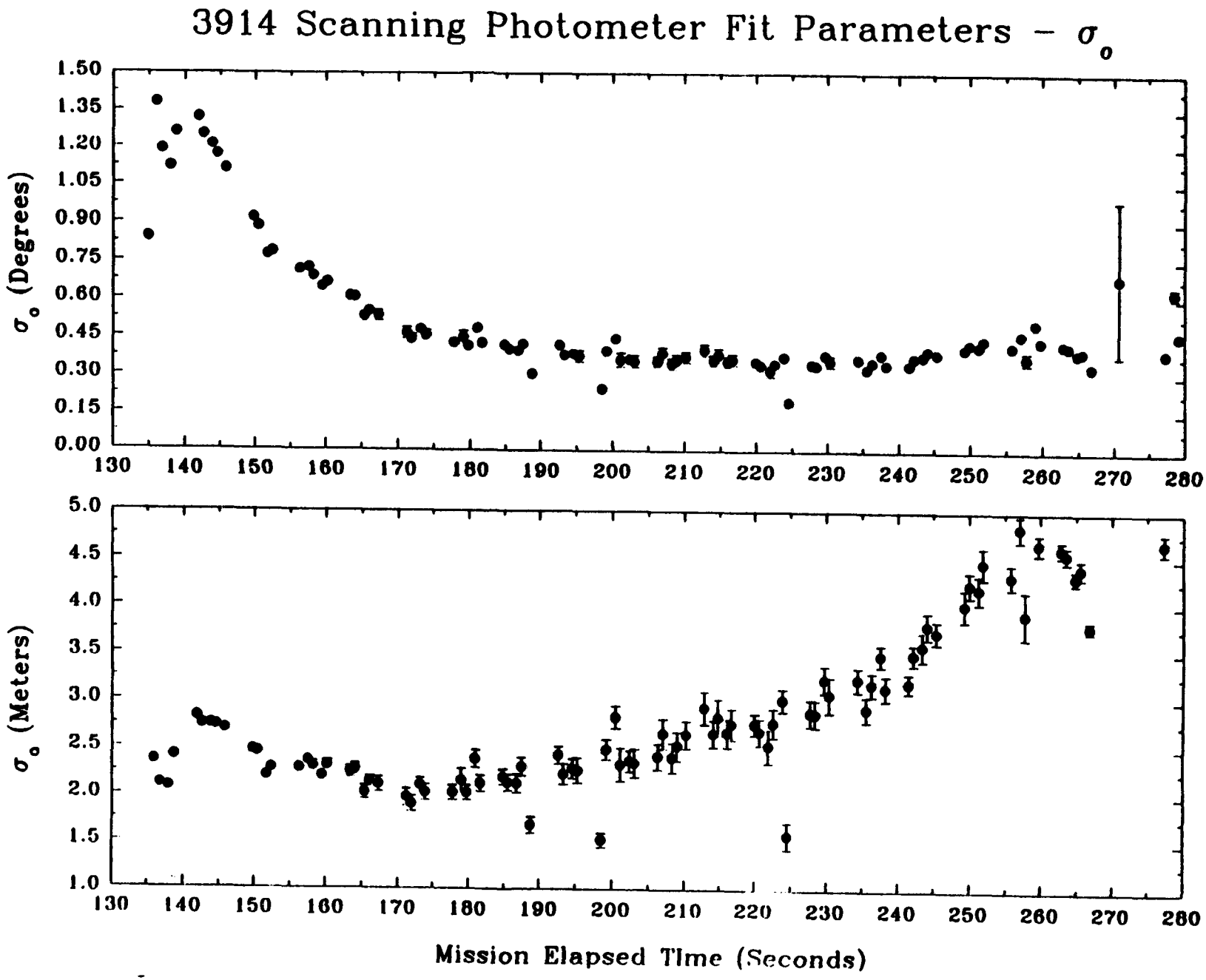

Figure 9. 3914 Å scanning photometer fit parameters - generalized width (in units of meters and degrees).

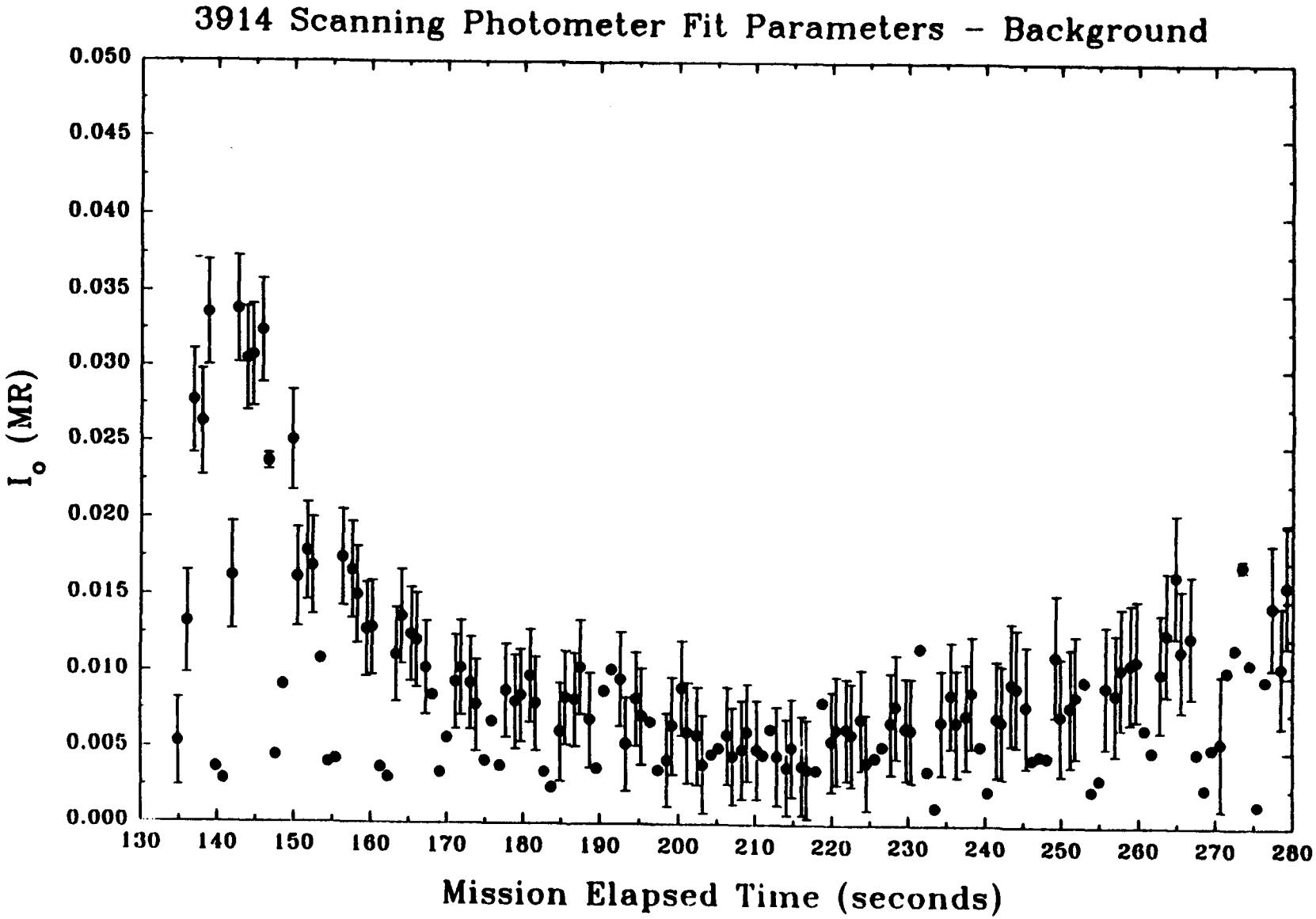

Figure 10. 3914 Å scanning photometer fit parameters - background.

The fitted background intensity is plotted in Figure 10 and the background with the beam on tends to be proportional to the integrated 3914 Å signal characterized by A_Σ throughout the flight. This is to be compared with the beam off scans which have a nearly constant intensity ($\sim$0.004 MR) independent of time or altitude. The background at 3914 Å is $\sim$0.006 MR near apogee which corresponds to $\sim$196 counts/seconds or $\sim$5 times the dark noise of the photomultiplier detector. This difference may be caused by scattered light inside the photometer or may be an artifact of the fit.

Transmission. The spectral response of the narrow band filter used in the photometer is gaussian in shape whereas the spectral shape of the 3914 Å emission is asymmetric with a short wavelength tail resulting from its band structure. Consequently, the filter does not cover the entire spectral region of the 3914 Å emission and the spectral "efficiency" must be calculated. Figure 11 shows a plot of the transmission of the filter and the N_2^+ spectral scan at 205 seconds (114.5 km). The spectral efficiency ϵ is calculated by

$$\epsilon(z) = \frac{\int I_{3914}(\lambda,z) \cdot T_{filter}(\lambda)\, d\lambda}{\int I_{3914}(\lambda,z) \cdot T_{peak}\, d\lambda} \qquad (15)$$

where z is the altitude and $I_{3914}(\lambda)$ is the spectral band profile. If $T_{filter}(\lambda)$ had the shape of a top hat and encompassed the entire 3914 peak, ϵ would be equal to 1.

Fourteen visible spectrometer scans were used to determine the value of ϵ. The integral over the N_2^+ band was carried out numerically by simply summing the spectral bins between the wavelength region from 3870 Å to 3940 Å. The value for ϵ showed no significant systematic variations over the 14 independent evaluation and were therefore averaged together to obtain a value of 0.546 ± 0.012. This represents the fraction of the N_2^+ emission that was observed; the entire 3914 Å data was then scaled by $1/\epsilon$.

Comparison with Photographic Data. Three data scans from the 3914 Å scanning photometer were compared with similar scans derived from a photographic analysis made by Photometrics, Inc.. Scans intended to represent the overall flight were chosen at the following times: 152 seconds (pulse 5), 201.7 seconds (pulse 12), and 258.5 seconds (pulse 20). The results are shown in Figures 12, 13, and 14. The solid line is the fit to the scanning photometer data by a generalized gaussian function; the points are data points from a micro-densitometer scan of the photographic data. The amplitudes are relative and were scaled for the comparison. The agreement of the shapes at 152 and 201.7 seconds is impressive and provides confidence in the measurement of the energy deposition. The disagreement in the two data sets at 258.5 seconds is likely due to the two instruments viewing different locations on a rapidly changing beam. It is also noted that the amplitudes from the two measurements have been reconciled and agree to better than 15 percent. Additional analysis of the photographic data is being done and will be reported elsewhere.

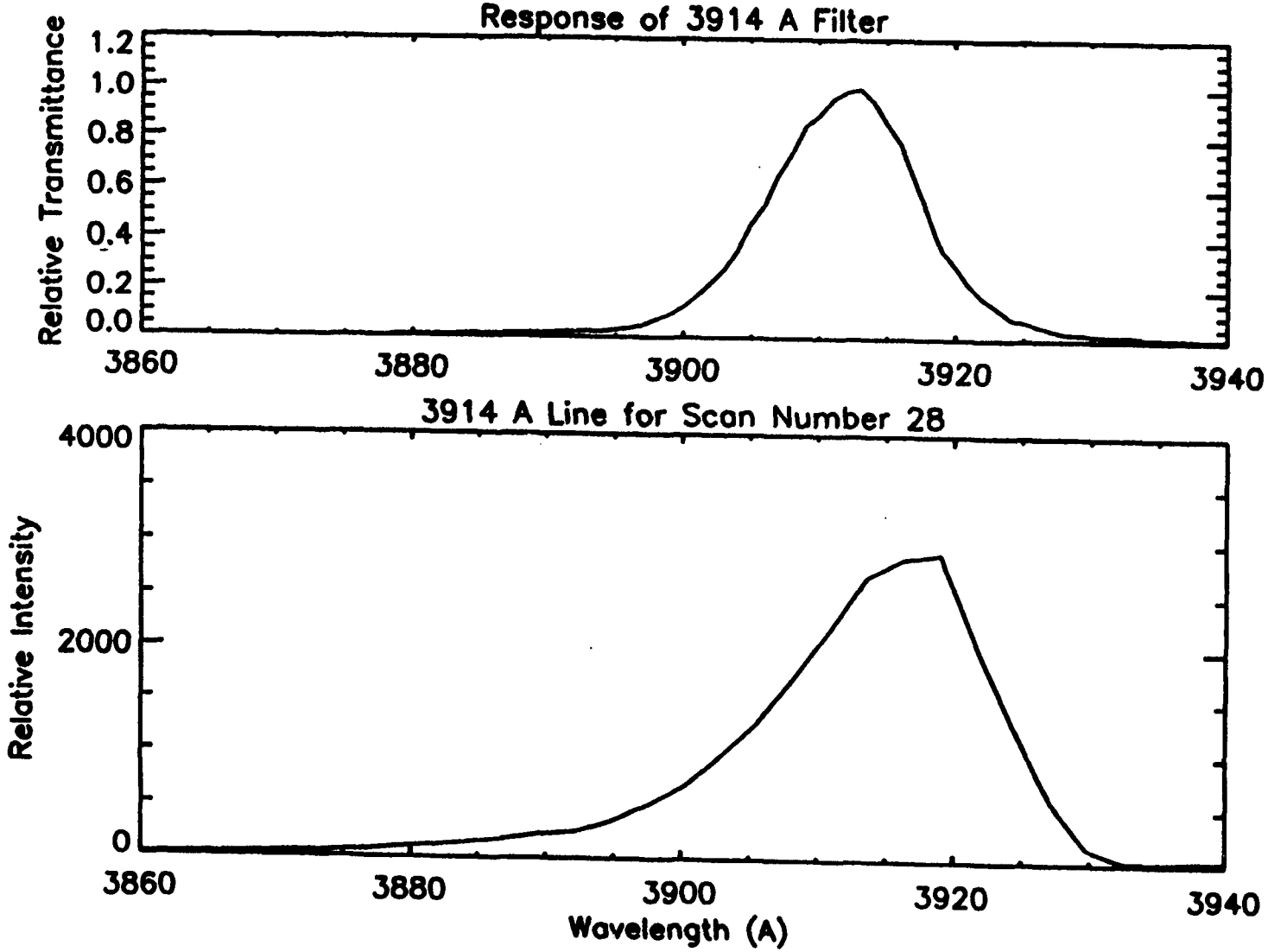

Figure 11. Transmission curve for 3914 Å scanning photometer.

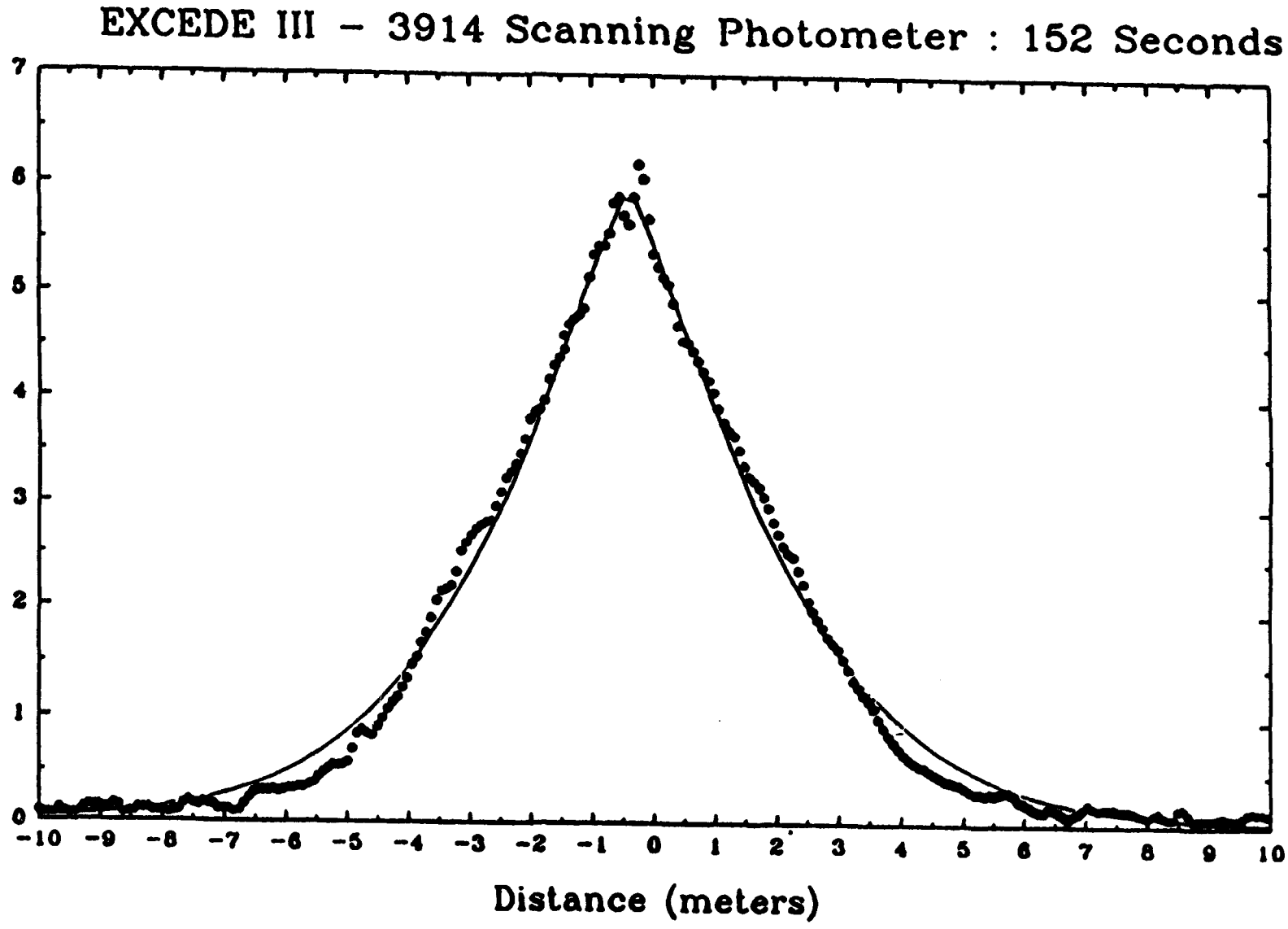

Figure 12. Comparison of scanning photometer data with photographic data at 152 s.

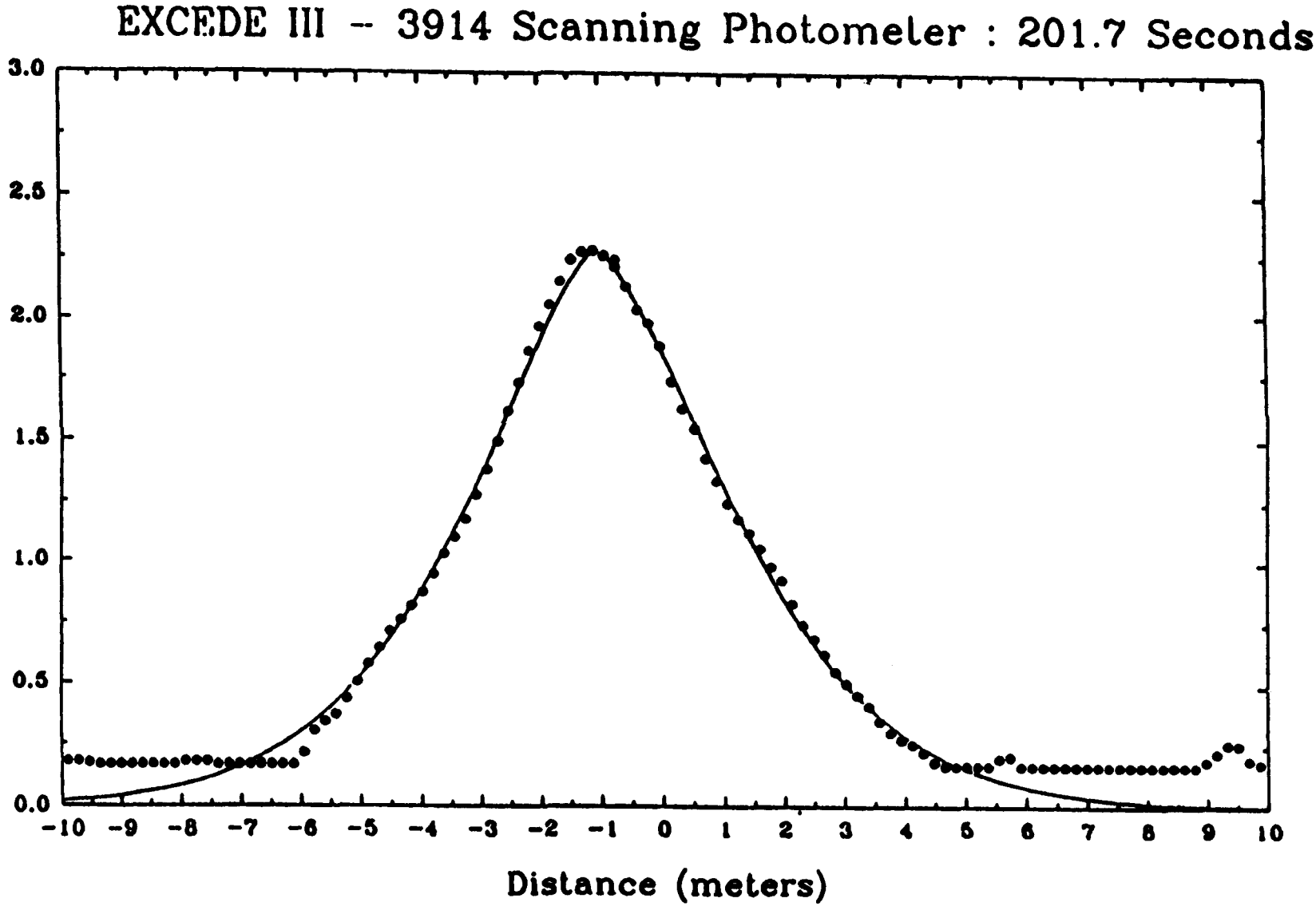

Figure 13. Comparison of scanning photometer data with photographic data at 201.7 s.

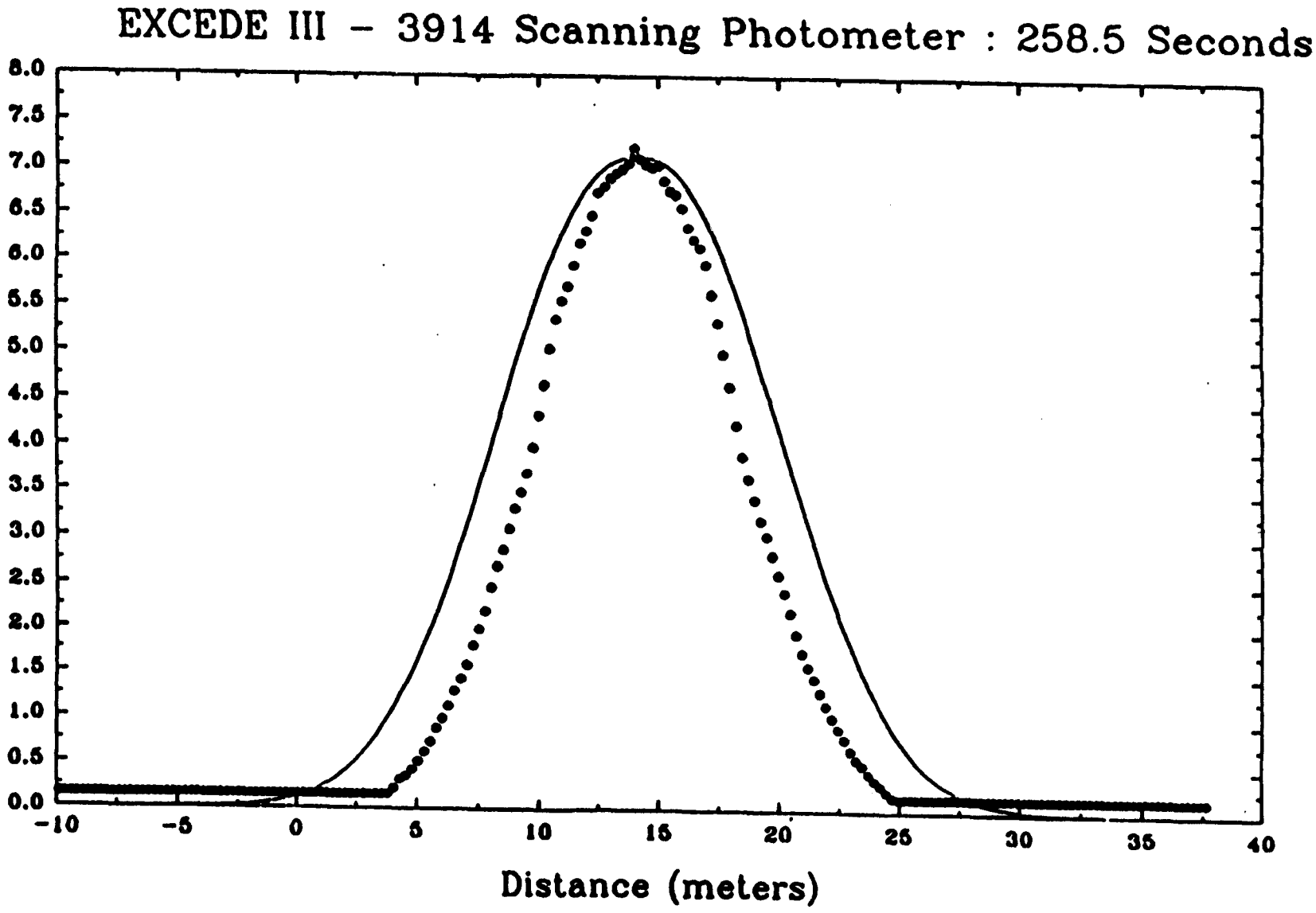

Figure 14. Comparison of scanning photometer data with photographic data at 258.5 s.

Analysis

We have obtained good fits for ~40 scans prior to apogee and for ~40 past apogee (apogee was 115 km and occurred 195 s into the flight).

One possible way to characterize the measured width of the beam is to compute the RMS radius. This characterization is independent of the exponent (other characterizations such as FWHM are not) and represents the point where half of the integrated power is within that distance and half of the power lies outside of that dimension.

The RMS radius is defined as the second moment of the distribution and is described by the expression (see Appendix A.)

$$\langle r^2 \rangle \equiv \frac{\int_0^\infty \rho(r)\, r^3\, dr}{\int_0^\infty \rho(r)\, r\, dr} = \sigma^2\, (2p^{2/p})\, \frac{\Gamma(3/p)}{\Gamma(1/p)} \qquad (16)$$

The RMS radius is plotted as a function of altitude in Figure 15 and remained relatively constant above ~ 102 km, ranging between ~4 and 5 meters. The increase in the beam radius seen at lower altitudes is due to viewing the beam at a larger fraction of the practical range during this portion of the flight. The beam diameter is increased because of the larger number of collisions.

The atmospheric dosing from the EXCEDE III beam has been calculated. The beam is an extended source and consequently the dose is different at different points across the beam. The dose is related to the energy deposition by

$$D(y,t) = \frac{\Sigma(y,t)}{v_\perp}$$

where $\Sigma(y)$ is the energy deposition as determined from the 3914 Å scanning photometer and $v_\perp$ is the velocity component of the accelerator module transverse to the local magnetic field.

The number of detected 3914 Å photons can be related to the energy deposition by noting that for every 3914 Å photon there are ~14.1 N_2^+ ions created [*Borst and Zipf*, 1970]

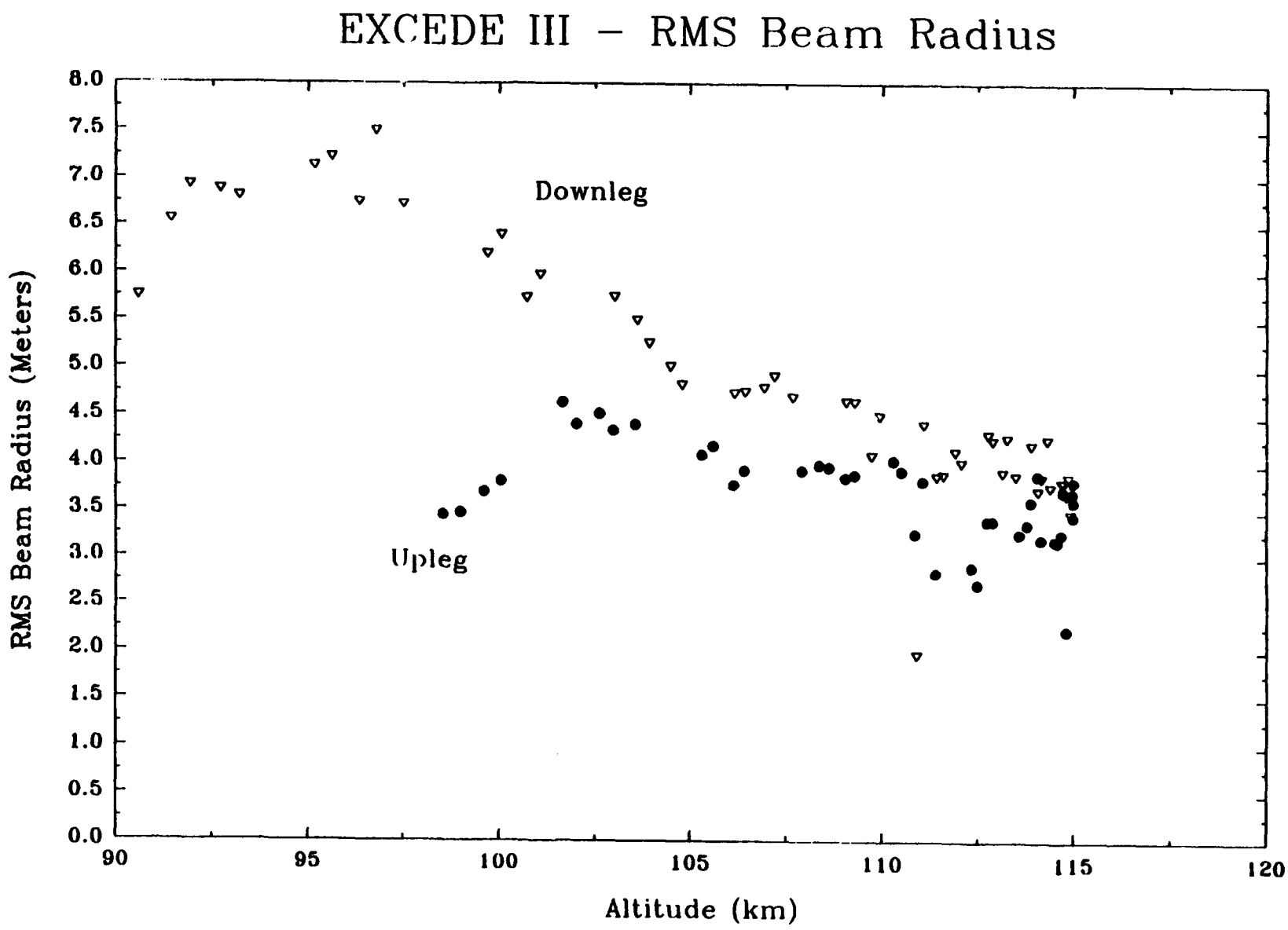

Figure 15. Plot of RMS radius derived from 3914 Å scanning photometer data.

(assuming the electron energies are in excess of -50 eV). The fraction of ion pairs that produce N_2^+ ions is given by [*Rees and Jones*, 1973]

$$\textit{ionization fraction} = \frac{0.92\ [N_2^+]}{1.15\ [N_2^+]+1.5\ [O_2^+]+0.56\ [NO^+]} \tag{18}$$

and each ion pair has associated with it the local deposition of -35 eV of energy.

An average dosing rate can be calculated assuming the RMS beam diameter as a characteristic width for the beam. The average dosing rate is given by

$$\langle D(t) \rangle_y = \frac{1}{v_\perp} \frac{\int \Sigma(y,t)\ dy}{\langle y \rangle} \tag{19}$$

This quantity is easily calculated by noting that the integral over the distribution $\Sigma(y)$, is equal to the fit parameter A_Σ.

$$A_\Sigma \sin\theta = \int_{-\infty}^{\infty} \Sigma_p'(y)\ dy = 2\pi \int_0^{\infty} \rho(r)\ r\ dr \tag{20}$$

The average dose is calculated by dividing A_Σ by $v_\perp$ and the RMS diameter. A plot of the average and peak dosing rates is shown in Figure 16.

The maximum dose is reached on upleg at ~ 102 km and is in excess of 10^{13} eV/cm^3. The value of the dose gets smaller all the way up to apogee where it is a minimum ($\sim 3.5 \times 10^{10}$ eV/cm^3) and then increases as the altitude decreases.

Caution is required when considering the maximum dose values. Let $(dP/dx)_s$ be the energy deposited per second along the beam at a distance s from the accelerator. The assumption is made for the above calculations that the value for dP/dx is approximately constant close to the scanned region. This is a very good approximation for the majority of the flight where the dose time is short and the accelerator module moves very little in the beam direction. Under these conditions the scanned region is dosed by the portion of the beam approximately a distance s_o along the beam. This is *not* true where the dose time is a maximum. In that case almost all of the motion is along the beam direction and therefore the irradiated volume is exposed to an energy deposition rate, $(dP/dx)_s$ at many different values of s on the beam which varies significantly.

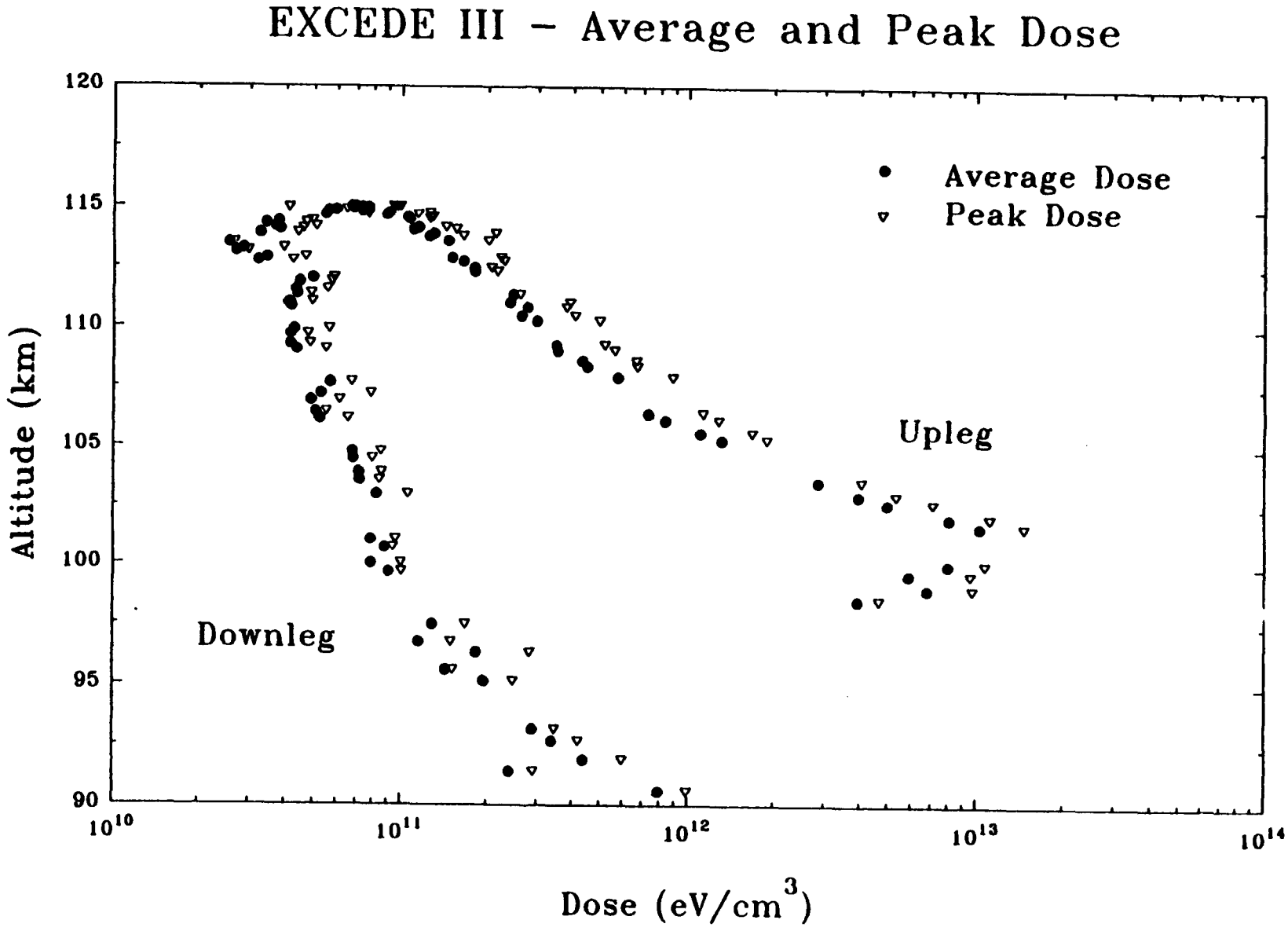

Figure 16. Plot of the average and peak dose derived from 3914 Å scanning photometer data.

Similarly, an average surface brightness for the 3914 Å emission can be calculated by the following expression

$$B_{3914} = \frac{A_\Sigma \sin\theta}{4\pi\ 2r_{RMS}} \frac{hc}{\lambda} \tag{21}$$

Catalog. A table of all fit parameters have been compiled for all scans and is presented in Appendix B. in addition to the relevant fit parameters and the associated errors, the RMS diameter and dosing for each scan has been included. Note that although a secondary gaussian (p=2) was fit where possible, *the primary peak is taken to describe the beam deposition.*

Plots of the data and the corresponding fit are shown in Appendix C. Each scan is displayed on a linear scale in the upper plot and a logarithmic scale in the lower plot. Plots with unusually large values for p (e.g. scan number 1.) correspond to incomplete scans where the beam was either turned on or off during the data collection.

A floppy disk containing the Appendix B and the data set presented in Appendix C has also been produced.

Calculating the Abel Transform. In many cases the integrated line scan across the beam, A_Σ is adequate for a particular application (e.g. calculating an auroral efficiency). For others, however, the derived radial distribution is necessary. In the latter case the corresponding inverse Abel transform must be calculated. A method is described below for extracting the value of the radial distribution at a point r for a given scan. The following approach reduces the expression to a dimensionless quantity described by a family of curves.

Each spatial scan from the 3914 Å scanning photometer has been fit to a generalized gaussian distribution and can be inverted using the inverse Abel transform to obtain the radial distribution. The radial distribution can be expressed in the generic form

$$\rho(r) = \frac{A_\Sigma}{2\pi\sigma^2} \sin\theta\ P(\frac{r}{\sigma},p) \tag{22}$$

The parameters A_Σ, σ, p, $\sin\theta$, and the generalized exponent p are listed in Appendix B for each scan along with other parameters.

As an example of this method consider pulse 4 at t=136.83 seconds. What is the value of ρ at a distance of 5 meters from the beam center? The corresponding value of the fit parameters at t=136 seconds are

$$A_\Sigma = 198.86 \text{ MR-meter}$$
$$\sigma = 2.11 \text{ meters}$$
$$p = 1.40$$
$$\sin\theta = 0.69$$
$$r/\sigma = 2.37$$

Figure 17 shows a family of curves of $P(r/\sigma,p)$ for different values of p; specific values of $P(r/\sigma,p)$ can be obtained from this plot. The value of P(2.37,1.40) is found to be equal to 0.073 from Figure 17. The value for ϵ is

$$\rho(2.37) = \frac{(198.86)}{(2\pi)\ (2.11 \times 10^2\ cm)^2}\ (0.69)\ (0.073)\ MR\text{-}meters \times 100\ cm/meter \tag{23}$$

$$= 3.58 \times 10^9\ photons/cm^3\text{-}s$$

Note that the units are Megarayeigh-meters/cm^2 and have been converted to photons/cm^3-s.

The user may ultimately find it easier to calculate $P(r/\sigma,p)$ using the formulation

$$P(\frac{r}{\sigma},p) = \frac{p^{2-2/p}}{\Gamma(1/p)}\ \alpha^{1-1/p} \int_0^\infty \cosh^{p-1}v\ e^{-\alpha \cosh v}\ dv \tag{24}$$

where

$$\alpha = \frac{1}{p}\ (\frac{r}{\sigma})^p \tag{25}$$

which is computationally better behaved at r=0.

Figures 18 and 19 are plots of the energy deposition from the beam for the above fit parameters and are intended to characterize the overall beam profile. The Abel Transform has been calculated for the values p=1.40 and σ=2.11 meters (see scan number 46) and the resulting spatial distribution has been plotted as an image in Figure 18. Figure 19 is a 2-dimensional picture of the same cross sectional distribution.

Summary

The energy deposition from the EXCEDE III beam was monitored by observing the N_2^+(1N) emission at 3914 Å with a narrowband filter photometer that scanned across the beam each

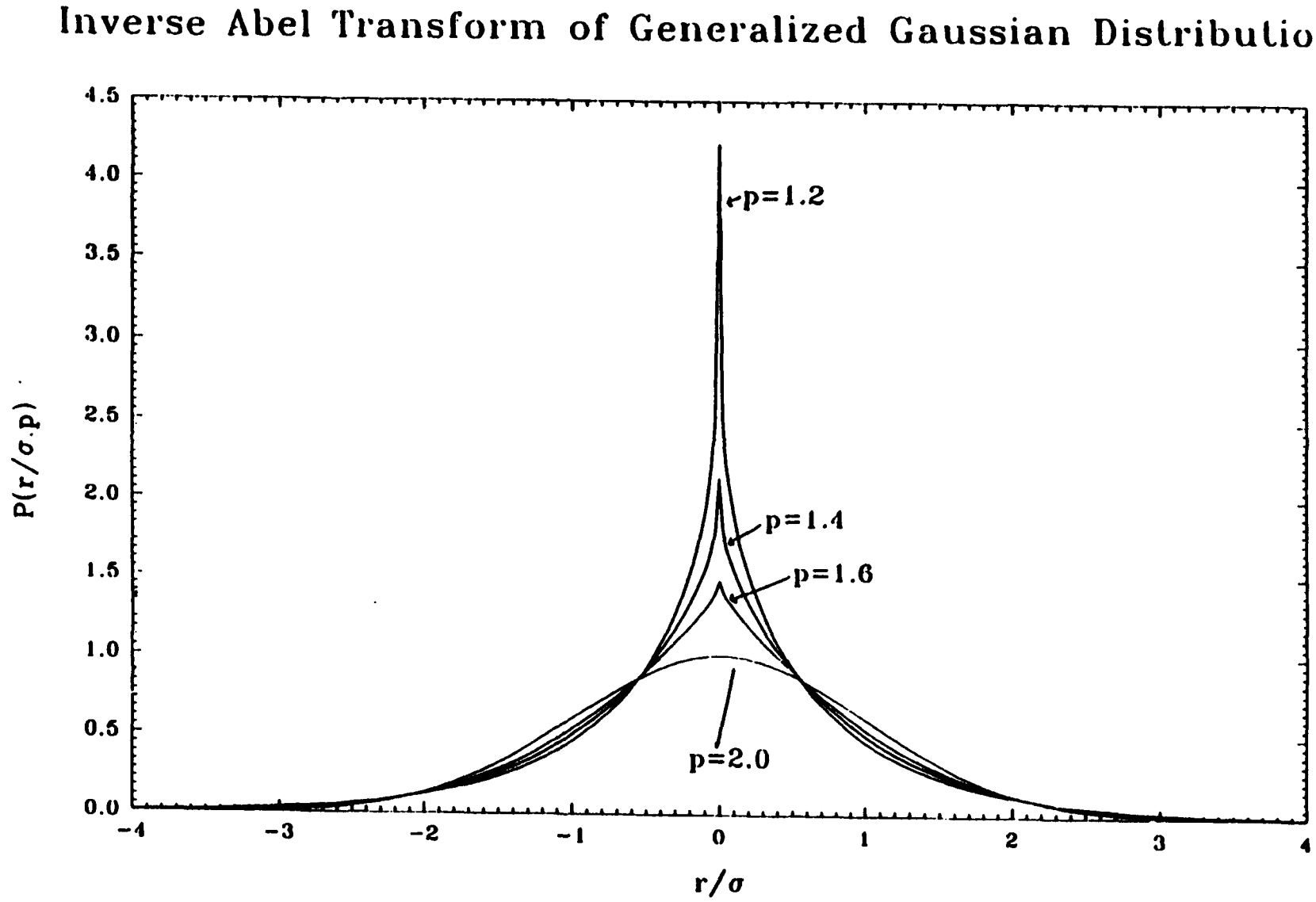

Figure 17. Plot of the family of curves P(r/σ), for calculating the inverse Abel transform.

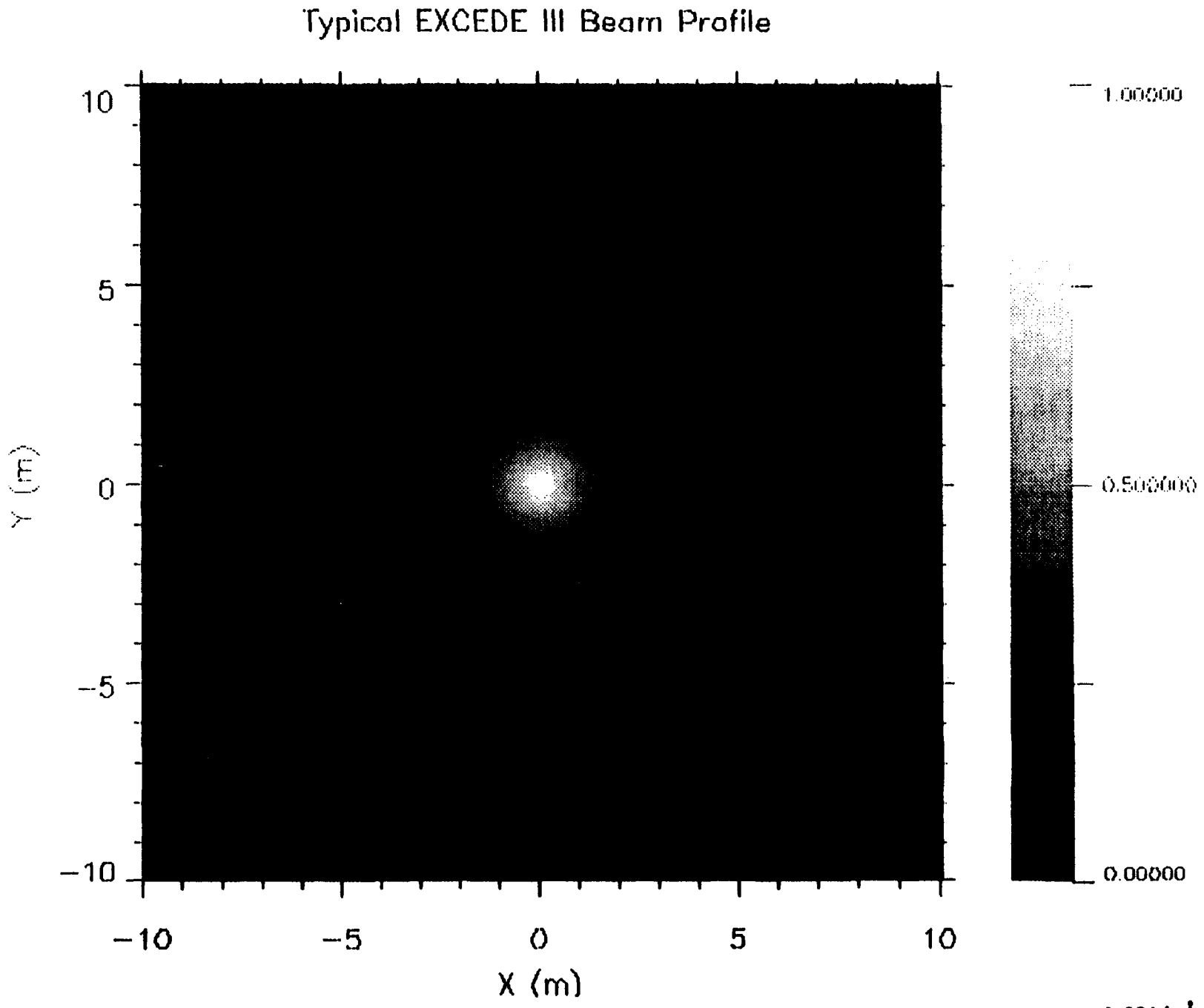

Figure 18. Image of the resulting spatial distribution of the energy deposition from a typical 3914 Å scanning photometer measurement.

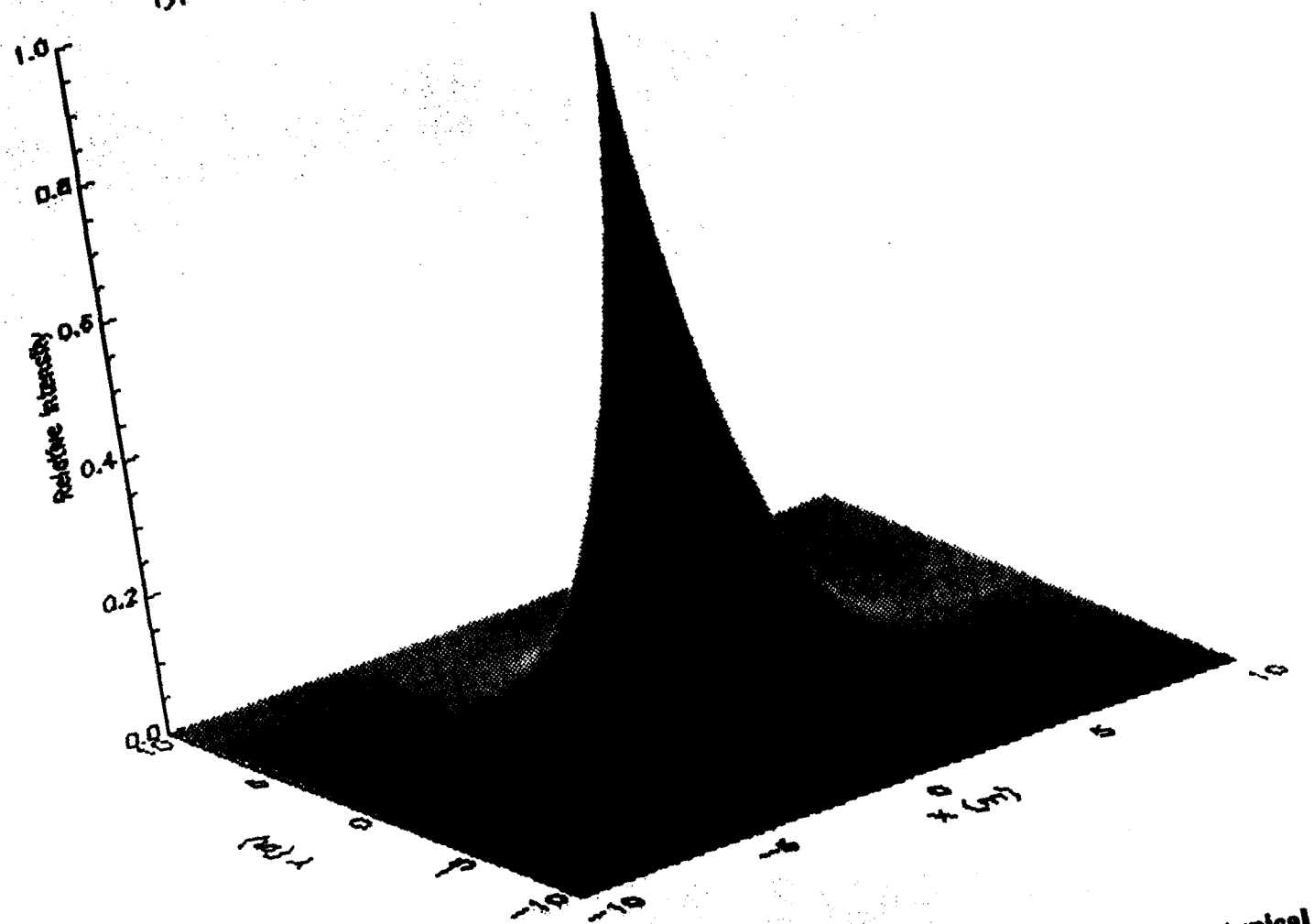

Figure 19. 2-dimensional plot of the spatial distribution of the energy deposition from a typical 3914 Å scanning photometer measurement.

second. Ninety (90) scans were collected with the beam on and were used to characterize the spatial deposition of the beam. Quality fits to the data were obtained using generalized Gaussian distributions. These distributions were then inverted by calculating the inverse Abel transform to obtain the corresponding radial distributions of the energy deposition.

The RMS radius for each scan of the beam has been calculated along with the average and peak dose which is in excess of 10^{13} eV-cm^{-3} near maximum dose.

Appendix A: Moments of the Distributions

It is convenient to describe the deposition profile in terms of the spatial moments of the profile. By making use of the definition of the Abel transform and changing the order of integration, several useful relationships can be derived. For

$$M_n \equiv \int_0^\infty y^n \, \Sigma_p'(y) \, dy \tag{26}$$

we obtain

$$M_n = \frac{A_\Sigma}{2} \frac{\Gamma(\frac{n+1}{p})}{\Gamma(\frac{1}{p})} (\sigma \, p^{1/p})^n \tag{27}$$

so that, in particular, $M_0 = 1/2$ and $M_p = 1/2 \, \sigma^p$. By making use of Eqn. (4) and using that with M_n as defined by Eqn. (25), we can obtain

$$\int_0^\infty y^n \, \Sigma_p'(y) \, dy = \frac{\sqrt{\pi} \, \Gamma(\frac{n+1}{2})}{\Gamma(\frac{n+2}{2})} \int_0^\infty \rho(r) \, r^{n+1} \, dr \tag{28}$$

It is now trivial to show that the rms radius of the deposition (r^2 averaged over the emissivity) is then given by

$$\langle r^2 \rangle \equiv \frac{\int_0^\infty \rho(r) \, r^3 \, dr}{\int_0^\infty \rho(r) \, r \, dr} = \sigma^2 \, (2p^{2/p}) \, \frac{\Gamma(3/p)}{\Gamma(1/p)} \tag{29}$$

References

Bevington, P.R., *Data Reduction and Error Analysis for the Physical Sciences*, McGraw-Hill Book Company, New York, 1969.

Borst, W.L., and E.C. Zipf, Cross section for electron-impact excitation of the (0,0) first negative band of N^+_2 from threshold to 3 keV, Phys. Rev. A, 1, 834-840, 1970.

Borst, W.L., and M. Imami, Production of secondary electrons in nitrogen by fast electrons and simultaneous excitation of N_2 bands, J. Appl. Phys., 44, 1133-1141, 1973.

Bracewell, R.N., Strip integration in radio astronomy, Aus. J. Phys., 9, 198-217, 1956.

Burns, D.J., F.R. Simpson, and J.W. McConkey, Absolute cross sections for electron excitation of the second positive bands of nitrogen, J. Phys. B, 2, 52-64, 1969.

Courant, R., and D. Hilbert, *Methods of Mathematical Physics*, Eng. ed., p. 158, Interscience Publishers, New York, 1953.

Jobe, J.D., F.A. Sharpton, and R.M. St. John, Apparent cross sections of N_2 for electron excitation of the second positive system, J. Opt. Soc. Am., 57, 106-107, 1967.

Press, W.H., On estimating the unprojected luminosity density within a cluster of galaxies, Astrophys. J., 203, 14-22, 1976.

Eshelman, Von R., The radio occultation method for the study of planetary atmospheres, Planet, Space, Sci., 21, 1521-1532, 1973.

Jones, L.M., F.F. Fishback, and J.W. Peterson, Satellite measurements of atmospheric structure by refraction, Planet. Space Sci., 9, 351-352, 1962.

Rees, M.H., and R.A. Jones, Time Dependent Studies of the Aurora-II: Spectroscopic Morphology, Planet. Space Sci., 21, 1213-1235, 1973.

Smith, G.R., and D.M. Hunten, Study of planetary atmospheres by absorptive occultations, Rev. Geophys., 28, 117-143, 1990.

Tarantola, A., *Inverse Problem Theory*, Elsevier, New York, 1987.